NANO EXPRESS

Open Access

CrossMark

Effects of Bilayer Thickness on the Morphological, Optical, and Electrical Properties of Al₂O₃/ZnO Nanolaminates

Da-Hai Li[1], Chen-Hui Zhai[1], Wen-Chao Zhou[2], Qing-Hua Huang[3], Lei Wang[3], Hua Zheng[1], Lei Chen[3], Xin Chen[4] and Rong-Jun Zhang[1*]

Abstract

This report mainly focuses on the investigation of morphological, optical, and electrical properties of Al₂O₃/ZnO nanolaminates regulated by varying bilayer thicknesses. The growth mechanism of nanolaminates based on atomic layer deposition and Al penetration into ZnO layer are proposed. The surface roughness of Al₂O₃/ZnO nanolaminates can be controlled due to the smooth effect of interposed Al₂O₃ layers. The thickness, optical constants, and bandgap information of nanolaminates have been investigated by spectroscopic ellipsometry measurement. The band gap and absorption edge have a blue shift with decreasing the bilayer thickness on account of the Burstein-Moss effect, the quantum confinement effect and the characteristic evolution of nanolaminates. Also, the carrier concentrations and resistivities are found to be modified considerably among various bilayer thicknesses. The modulations of these properties are vital for Al₂O₃/ZnO nanolaminates to be used as transparent conductor and high resistance layer in optoelectronic applications.

Keywords: Al₂O₃/ZnO nanolaminates, Atomic layer deposition, Morphological properties, Optical properties, Electrical properties

Background

Nanolaminate is a composite structure formed by different stacking sequences of diverse materials, and the layer thickness is general at the nanometer scale [1–4]. This multi-layered structure can endow the nanolaminate with unique properties, and these properties depend on or may be better than those of the constituent materials [5–7]. In recent years, a new kind of materials based on the structure of nanolaminate is began to be utilized for energy storage devices [8], innovative optical elements [9], and temperature sensitive substrates for biosensors [10]. Recently, Viter et al. explored on the tuning of structural properties and the enhancement of electronic and optical properties of 1D PAN (polyacrylonitrile) ZnO/Al₂O₃ nanolaminates which will allow applications in different fields such as sensors and biosensors [11]. Baitimirova et al. also investigated the tuning of structural and optical properties of graphene/ZnO nanolaminates which may find applications in optical, bio-, and chemical sensors [12].

As one of the most promising candidates for transparent conductive oxide (TCO) materials, Al-doped ZnO (AZO) film has many advantages, such as abundant resource, low cost, nontoxicity, and good stability in hydrogen plasma. In general investigations, controlling the Al doping level is a common method to improve and modify the optical and electrical behaviors of AZO materials [13, 14], which is crucial to achieve functionalization and tunability of TCO-based devices [15, 16]. However, few reports involve in the performance modulation of AZO by changing the structures of Al₂O₃/ZnO nanolaminates which is more simple and effective in semiconductor manufacturing process.

The atomic layer deposition (ALD) technique is suitable for fabricating nanolaminate structures for different purposes and applications [17–19]. This technique is based on self-limiting surface chemical reactions with excellent deposition effect, which can make the thicknesses of individual nano-layers well-controlled for the composite stack. Furthermore,

* Correspondence: rjzhang@fudan.edu.cn
[1]Key Laboratory of Micro and Nano Photonic Structures, Ministry of Education, Department of Optical Science and Engineering, Fudan University, Shanghai 200433, China
Full list of author information is available at the end of the article

Li *et al. Nanoscale Research Letters* (2017) 12:563

Page 2 of 9

between different sublayers, good nucleation and adhesion can be realized by designing the surface reactions. Therefore, high-quality nanolaminates with uniform and smooth surface can be realized by ALD technique, and the thickness can be controlled accurately as well.
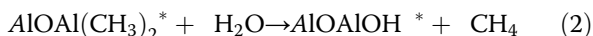
In this work, Al_2O_3 and ZnO materials were adopted to realize the nanolaminate structures in order to investigate the tunable characteristics of AZO by changing the bilayer thickness of Al_2O_3/ZnO nanolaminates. We investigate their morphological, optical, and electrical properties. The growth mechanism of nanolaminates and Al penetration into ZnO layer are proposed and discussed. With decreasing bilayer Al_2O_3/ZnO thickness in the nanolaminates, blue shift of the bandgap is observed and discussed on the basis of the Burstein-Moss (BM) effect, the quantum confinement effect, and the characteristic evolution of the nanolaminates. The tunable electrical properties are exposed by using a measurement system based on the Hall effect. It gives valuable references and ideas that transparent conductor and high-resistance layer can be achieved by varying the bilayer thickness in the nanolaminates.
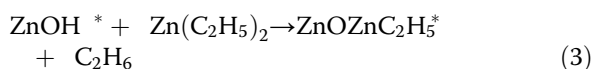
Methods

Synthesis of Nanolaminates by ALD

Al_2O_3/ZnO nanolaminates based on Al_2O_3-ZnO bilayer stacks were deposited on SiO_2/Si and quartz substrates by ALD technique. During deposition procedure, the reactor (PICOSUN) temperature was 150 °C. The precursors for Zn, Al, and O were diethylzinc [DEZ; $Zn(C_2H_5)_2$], trimethylaluminum [TMA; $Al(CH_3)_3$], and deionized water (H_2O), respectively. The precursor carrier and purge gas was the high purity nitrogen (N_2, flow rate 50 sccm). It was used to carry precursors into the chamber and bring the needless products out of the chamber.

In order to grow the Al_2O_3 layers, the TMA and H_2O were alternatively brought into the reactor chamber through TMA-H_2O cycles (TMA/exposure/N_2/H_2O/exposure/N_2) with pulse time of 0.03/3/15/0.03/5/15 s. The surface reactions of ALD Al_2O_3 layers can be defined by two self-limiting reactions as follows [20]:

$$AlOH^* + Al(CH_3)_3 \rightarrow AlOAl(CH_3)_2{}^* + CH_4 \quad (1)$$

$$AlOAl(CH_3)_2{}^* + H_2O \rightarrow AlOAlOH^* + CH_4 \quad (2)$$

where the asterisks indicate the surface species. As for ZnO layers, DEZ-H_2O cycles of ZnO were the same as the TMA-H_2O. The surface reactions of ALD ZnO layers are given by [20]

$$ZnOH^* + Zn(C_2H_5)_2 \rightarrow ZnOZnC_2H_5{}^* + C_2H_6 \quad (3)$$

$$ZnOZnC_2H_5{}^* + H_2O \rightarrow ZnOZnOH^* + C_2H_6 \quad (4)$$

where the asterisks also indicate the surface species. The

structure diagram of ALD Al_2O_3/ZnO nanolaminates is shown in Fig. 1. For all nanolaminates, the interface with the substrate was Al_2O_3, while ZnO was the top layer at the surface of nanolaminates. The bilayer is constructed by two individual layers, i.e., Al_2O_3 and ZnO, with the same thickness. In order to guarantee the same thicknesses of total nanolaminates, the number of bilayer was increased with the decrease of bilayer thickness. So five kinds of samples were prepared, named as 2 (25/25 nm), 5 (10/10 nm), 10 (5/5 nm), 25 (2/2 nm), and 50 (1/1 nm). The details can be found in Table 1. Note that the parameters in Table 1 are the empirical values, which are summarized from our preliminary experiments.

Characterization

The morphological characterization of Al_2O_3/ZnO nanolaminates was carried out by transmission electron microscope (TEM; FEI Tecnai G2 F20) and atomic force microscopy (AFM; Bruker Dimension Icon VT-1000, Santa Barbara, CA). The thickness, optical constants, and bandgap information were determined by spectroscopic ellipsometry (SE; J.A. Woollam, Inc., M2000X-FB-300XTF) measurements in the wavelength range of 200–1000 nm under an incident angle of 65°. The optical transmittance of nanolaminates has also been studied in the wavelength range of 200–1000 nm by using a dual beam spectrophotometer (Shimadzu UV-3600). A Hall effect measurement system (Ecopia HMS3000) was used to obtain electrical properties of the samples with a four-point probe.

Results and Discussion

Morphological Characteristics

Nanolaminates with different bilayer thicknesses grown on SiO_2/Si substrates were measured on cross sections with TEM. Three illustrative examples of nanolaminates with a bilayer thickness of 50, 10, and 2 nm are shown in Fig. 2, including the high-magnification images of 50- and 10-nm samples. Clear boundaries can be observed between Al_2O_3 and ZnO layers, and the thickness of total nanolaminates is indicated. With the help of X-ray diffraction (Bruker D8
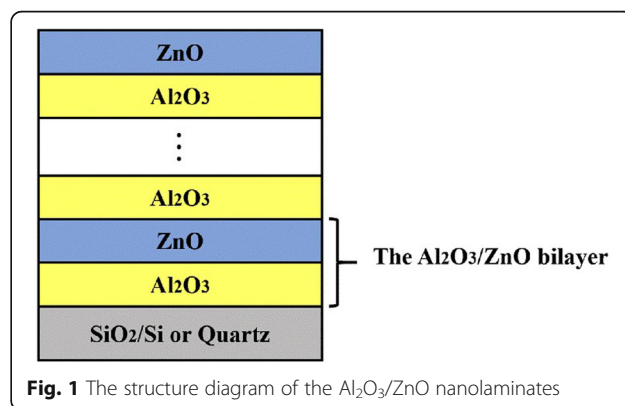

Fig. 1 The structure diagram of the Al_2O_3/ZnO nanolaminates

Li *et al. Nanoscale Research Letters* (2017) 12:563

Page 3 of 9

Table 1 The parameters of samples with different bilayer thicknesses

Sample	Layer thickness (nm)		Cycles		The number of bilayer
	Al_2O_3	ZnO	Al_2O_3	ZnO	
2 (25/25 nm)	25	25	250	150	2
5 (10/10 nm)	10	10	100	60	5
10 (5/5 nm)	5	5	50	30	10
25 (2/2 nm)	2	2	20	12	25
50 (1/1 nm)	1	1	10	6	50

ADVANCE) measurements in advance (not given here), we find no characteristic peaks of Al_2O_3 and ZnO, and hence that all of the as-grown nanolaminates have amorphous state. This statement can be verified by the high-magnification TEM images. Even though Al_2O_3/ZnO 2 (25/25 nm) samples have the thickest bilayer in this work, the crystallization process does not exist in them.

As reported elsewhere [6, 21], the Al_2O_3 layer in Al_2O_3/ZnO nanolaminates prepared by ALD method is always in amorphous phase and it can block the ZnO crystal growth because the ZnO is forced to renucleate on the Al_2O_3 surface. The crystallization process of ultrathin layers is very complex, and many factors should be taken into account, such as the interface energies, the thickness of the layers, the melting point of the system, and the bulk amorphous crystallization temperature [6, 22]. Viter et al. discovered that Al_2O_3/ZnO nanolaminates with bilayer thickness of 20 nm (ratio 1:1) have amorphous nature and they attributed this result to the minimum thickness required to allow crystallization [22]. López et al. found similar phenomenon and they thought that the pulse as well as the purge

duration of the growth procedure was too short to give their films enough time for generating some ordering and some crystalline phases [23]. Meanwhile, the Bohr radius of bulk ZnO is 23 Å [4]. Al_2O_3/ZnO 25 (2/2 nm) and Al_2O_3/ZnO 50 (1/1 nm) nanolaminates have ZnO thicknesses smaller than the Bohr radius; therefore, the quantum confinement effect should be taken into consideration. Especially for semiconducting sublayers ZnO, it is believed that this effect can cause dramatic change in the dielectric behavior [21], and we will discuss it in the following content.

To investigate the surface morphologies of the nanolaminates, AFM measurement is applied for the samples deposited on SiO_2/Si substrates, and the 3D results are shown in Fig. 3. It can be observed that the hill-shaped features are dominated on the sample surface and surface height decreases with lower bilayer thickness. Samples with low bilayer thicknesses, i.e., Al_2O_3/ZnO 25 (2/2 nm) and Al_2O_3/ZnO 50 (1/1 nm), show smooth surface with insignificant surface roughness. The root-mean-square roughness R_q of each nanolaminate is estimated from AFM data and approximately ranges from 0.81 to 1.30 nm. Moreover, the relationship between bilayer thickness and R_q is revealed in Fig. 4. At first, the values of R_q show linear behavior vs. the increase of bilayer thickness, then it remains stable when the bilayer thickness increases to a certain value, as is the case for other studies [23, 24]. The Al_2O_3 in this work is in amorphous phase under the above growth condition, which has been proved in our previous report as well [25]. The amorphous Al_2O_3 layer is very smooth and conforms to the topography of underlying ZnO
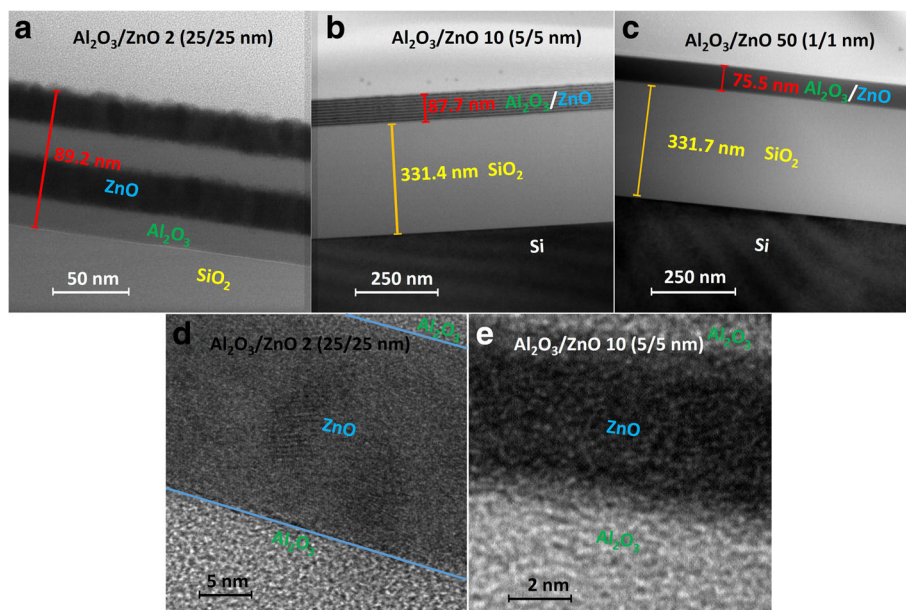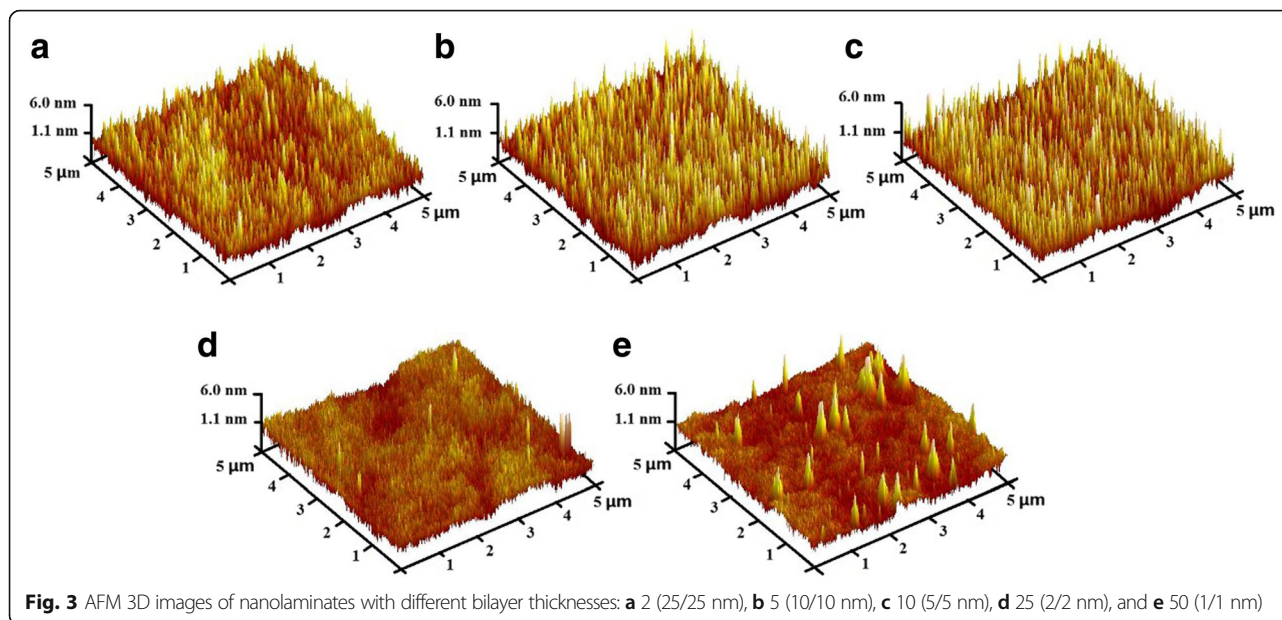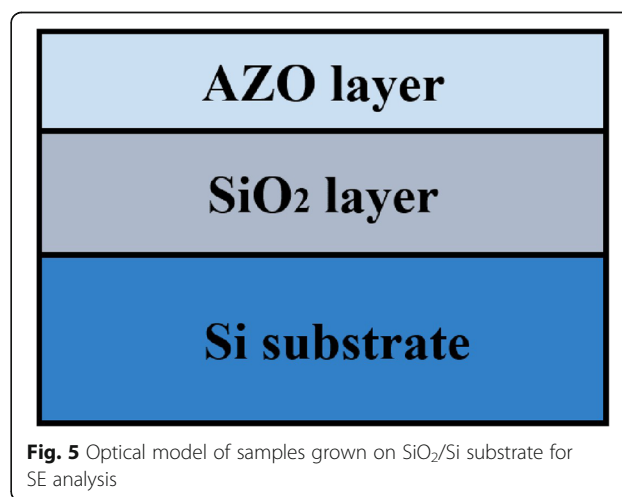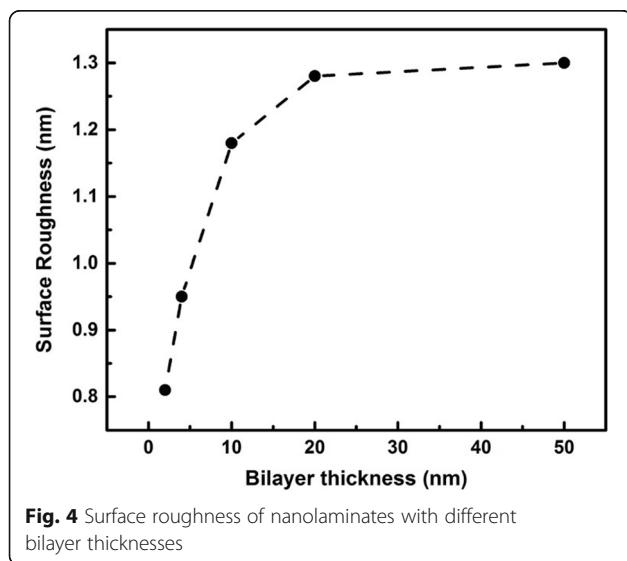

Fig. 2 TEM images of Al_2O_3/ZnO nanolaminates with different bilayer thicknesses: **a** 50 nm, **b** 10 nm, and **c** 2 nm. And high-magnification images: **d** 50 nm and **e** 10 nm

Li et al. Nanoscale Research Letters (2017) 12:563

Page 4 of 9

Fig. 3 AFM 3D images of nanolaminates with different bilayer thicknesses: **a** 2 (25/25 nm), **b** 5 (10/10 nm), **c** 10 (5/5 nm), **d** 25 (2/2 nm), and **e** 50 (1/1 nm)

layers [26]. As mentioned above, due to the interposed Al_2O_3 layer, the crystal growth of ZnO is consequently interrupted. Through restricting the size of the ZnO nanocrystals, the interposed Al_2O_3 layers prevent the Al_2O_3/ZnO nanolaminates from roughening [24]. This smooth effect has been proven to have little to do with the Al_2O_3 layer thickness and only relates to the number of interposed Al_2O_3 layers [24]. Therefore, with the decrease of bilayer thickness, more Al_2O_3 layers were interposed into the nanolaminates to smooth roughness, which leads to the nanolaminates more smooth. When the bilayer thickness increases to a certain value, this smooth effect is no longer obvious.

Optical Properties

By performing SE measurement [17, 27, 28] which is based on recording and calculating the change of a reflected linearly polarized light from the surface of samples, the optical constants and film thickness of nanolaminates can be deduced from the raw data. In order to get more accurate details, the nanolaminates grown on SiO_2/Si substrates are chosen as the testing object because of its opaque to light during SE measurements. After raw data acquisition, a multilayer model is constructed containing semi-infinite Si substrate, SiO_2 layer, and AZO layer, as revealed in Fig. 5. The nanolaminates, i.e., the AZO layer in the model, are considered as a whole to be fitted. Oxidation layer of Si substrate is about 330 nm, which is directly substituted into the model without fitting. Moreover, no Bruggeman effective media approximation is introduced in this optical model

Fig. 4 Surface roughness of nanolaminates with different bilayer thicknesses

Fig. 5 Optical model of samples grown on SiO_2/Si substrate for SE analysis

Li et al. Nanoscale Research Letters (2017) 12:563

Page 5 of 9

because of the ignorable surface roughnesses of samples based on the AFM results. On account of this optical model, the Forouhi-Bloomer (FB) dispersion model is used to fit the ellipsometry spectra (Ψ and Δ in the range of 200–1000 nm) of the nanolaminates [29, 30]. The final thickness and optical properties are fitted and evaluated to minimize the root-mean-square error (RMSE) which follows:

$$\text{RMSE} = \sqrt{\frac{1}{2N-M-1}\sum_{i=1}^{N}\left[\left(\psi_i^{\text{cal}}-\psi_i^{\text{exp}}\right)^2 + \left(\Delta_i^{\text{cal}}-\Delta_i^{\text{exp}}\right)^2\right]} \quad (5)$$

Here, N, M, exp, and cal represent the number of data points in the spectra, the number of variable parameters in the model, the experimental data, and the calculated data, respectively.

The fitted thicknesses of nanolaminates are shown in Table 2. They are very close to the values obtained from TEM measurements, indicating the accuracy of fitting process. The fitting error RMSE is also revealed in Table 2, and the value is within permitted, demonstrating the reliability of fitting results. The thicknesses of sample 2 (25/25 nm), 5 (10/10 nm), and 10 (5/5 nm) show a smooth trend, and the small fluctuation results from varying degrees of ALD surface chemical reactions. In contrast, the thicknesses of sample 25 (2/2 nm) and 50 (1/1 nm) decline obviously with decreasing bilayer thickness. It follows that the Al_2O_3/ZnO nanolaminates show different thickness with low bilayer thickness, even if the cycle number stays the same in deposition process. Table 3 summarizes the growth rates of Al_2O_3 and ZnO sublayers (thickness ratio 1:1) using the thicknesses listed in Table 2. The values increase at first and saturate finally when the cycles in sublayers increase. The variation in film thickness and growth rate may result from the interfacial reaction between Al_2O_3 and ZnO layers which will be introduced in the following content, and samples with lower bilayer thickness will be more affected. Karvonen et al. gave similar explanation, and they attributed the variation in growth rate to the TMA etching of ZnO during the Al_2O_3 growth [7]. Elam et al. found that the growth rates of Al_2O_3 and ZnO increase with the number of ALD cycles [24]. They concluded that the reduced growth rate of early ALD cycles may result from the nucleation process occurring when making the transition from Al_2O_3 to ZnO and from ZnO to

Table 2 The thicknesses of AZO layer obtained from TEM and fitted by SE, and the fitting error RMSE

Sample	Thickness$_{TEM}$ (nm)	Thickness$_{SE}$ (nm)	RMSE
2 (25/25 nm)	89.2	86.64	1.17
5 (10/10 nm)	–	88.18	0.83
10 (5/5 nm)	87.7	87.31	0.77
25 (2/2 nm)	–	80.90	0.69
50 (1/1 nm)	75.5	74.80	0.42

Table 3 The growth rates of samples with different bilayer thicknesses

Sample	Growth rate (Å/cycle) cycles			
	$Al_2O_{3\,TEM}$	ZnO_{TEM}	$Al_2O_{3\,SE}$	ZnO_{SE}
2 (25/25 nm)	0.89	1.49	0.87	1.44
5 (10/10 nm)	–	–	0.88	1.47
10 (5/5 nm)	0.88	1.46	0.87	1.46
25 (2/2 nm)	–	–	0.81	1.35
50 (1/1 nm)	0.76	1.26	0.75	1.25

Al_2O_3. Only when new crystals are formed does the growth rate achieve the steady state value.

The optical constants of Al_2O_3/ZnO nanolaminates are illustrated in Fig. 6. It shows various refractive index n and extinction coefficient k with different bilayer thicknesses. Figure 6a describes the refractive index dispersion spectra of the nanolaminates with different bilayer thicknesses. The values of n decrease gradually with decline of bilayer thickness in the range of 50 to 2 nm due to the growth change and the Al penetration [21, 31]. The $n(\lambda)$ characteristic of ZnO can be observed for nanolaminates with bilayer thicknesses of 50, 20, and 10 nm. And this line shape slowly degenerates and disappears when the bilayer thickness is below 4 nm. Consequently, the $n(\lambda)$ characteristics tend to behaving like Al_2O_3 as the sample 50 (1/1 nm) shown. The k dispersion spectra can be found in Fig. 6b. Different curves represent different samples with various bilayer thicknesses. In the region of 430–1000 nm, the extinction coefficients are approximately equal to 0, i.e., the nanolaminates are almost transparent in that wavelength region. Meanwhile, a blue shift occurs at the absorption edge with decreasing bilayer thickness. The shift distance of sample 25 (2/2 nm) and 50 (1/1 nm) is larger, so the absorption edge gradually moves out of the spectral region and presents the characteristics of Al_2O_3. As a whole, the characteristics of optical constants transfer from ZnO to Al_2O_3. The observed changes of n and k could be determined by two physical phenomena. On the one hand, they are affected by the quantum confinement effect. We can see that samples 25 (2/2 nm) and 50 (1/1 nm) have sublayer thicknesses smaller than the Bohr radius of bulk ZnO, so their dielectric behaviors change more dramatically than the other samples. On the other hand, it is based on the growth mechanism which leads to Al penetration into ZnO layers [22, 24]. According to the growth mechanism, the substitution reaction of Zn with Al may occur in the interface between ZnO and Al_2O_3 layers:

$$\text{Zn-OH}^S + \text{Al}(C_2H_5)_3{}^g\uparrow \rightarrow \text{AlOH-}C_2H_5{}^s + \text{Zn}(C_2H_5)_2{}^g\uparrow \quad (6)$$

where ZnO-OH and Al $(C_2H_5)_3$ are the substance on the surface and gas phase, correspondingly. Because of this interfacial reaction, Al doping into ZnO layers may
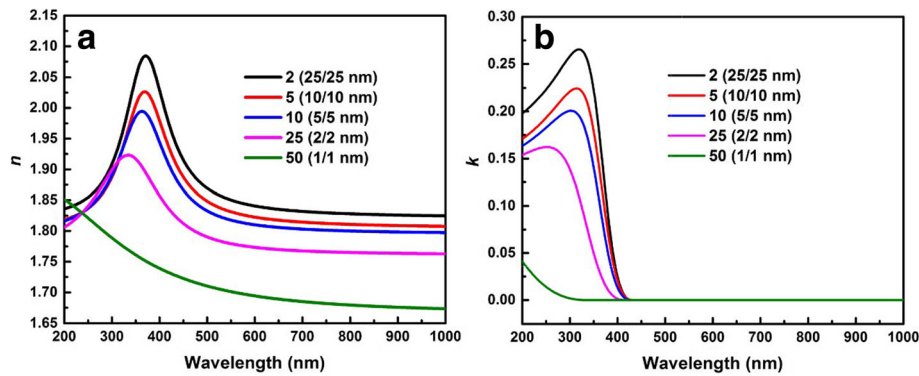
Li *et al. Nanoscale Research Letters* (2017) 12:563

Page 6 of 9

Fig. 6 The optical constants of nanolaminates grown on SiO₂/Si substrate. **a** The refractive index *n*. **b** The extinction coefficient *k*

happen and ZnO ratio in nanolaminates can be reduced. Therefore, with the decrease of the bilayer thickness, the interface between ZnO and Al_2O_3 layers increases, and the ratio of ZnO in the nanolaminates decreases accordingly. This can be verified by the high-magnification TEM images shown in Fig. 2d, e. When the bilayer thickness decreases, the boundaries between Al_2O_3 and ZnO layers become wider and blurrier. It makes the characteristic of whole nanolaminates transfers to that of Al_2O_3.

For better understanding of the blue shift of absorption edge, Tauc extrapolation is applied to evaluate the bandgap information of the nanolaminates with a bilayer thickness of 50, 20, and 10 nm. To evaluate the bandgap energies, extinction coefficients of the nanolaminates were used. Extinction, bandgap energy, and absorption coefficients are associated according to the following formulas [32]:

$$(\alpha h\upsilon)^2 = A(E - E_g) \tag{7}$$

$$\alpha = \frac{4k\pi}{\lambda} \tag{8}$$

where α is the optical absorption coefficient, A is a constant, and E_g is the optical bandgap energy. On the basis of Eqs. (7) and (8), a plot of $(\alpha h\upsilon)^2$ vs. $h\upsilon$ has been made as demonstrated in Fig. 7. The value of bandgap energy E_g can be graphically determined by x axis and the linear fitting in linear part of the absorption edge, which is provided in the inset figure of Fig. 7. The bandgap information of samples 25 (2/2 nm) and 50 (1/1 nm) is not revealed in Fig. 7, because the linear part of the absorption edge exceeds the spectral range evolved from the spectra of extinction coefficient, which could lead to inaccurate results. From Fig. 7, it can be seen that the bandgap energy of nanolaminate displays a growing trend with decreasing bilayer thickness, which could be interpreted by the BM effect [33–35]. Interposed Al^{3+} takes the place of Zn^{2+} in the interface of Al_2O_3/ZnO layers and provides an extra electron. So in nanolaminates, the concentration of free carriers increases, causing the bandgap energy

moves to higher energy region. The following equation can describe this effect exactly [35]:

$$E_g = E_g^0 + \Delta E_g^{BM} = E_g^0 + \frac{h^2}{8m_e^*}\left(\frac{3}{\pi}\right)^{2/3} n_e^{2/3} \tag{9}$$

where ΔE_g^{BM} and E_g^0 represent the increment of bandgap caused by BM effect and intrinsic forbidden bandwidth, while h, m_e^*, and n_e are the Plank's constant, effective electron mass in the conduction band, and electron carrier density, respectively.

Figure 8 gives the spectra of transmittance and absorbance of the whole group. It can be found that sharp absorption edges are located in the region from 200 to 400 nm, namely ultraviolet region. Importantly, absorption edges move to the shorter wavelength (blue shift) with decreasing bilayer thickness, and this trend is exactly close to previous results calculated from SE measurement. This blue shift is due to the BM effect that makes the increase of bandgap. However, the blue shift is not successional, because in the nanolaminates of
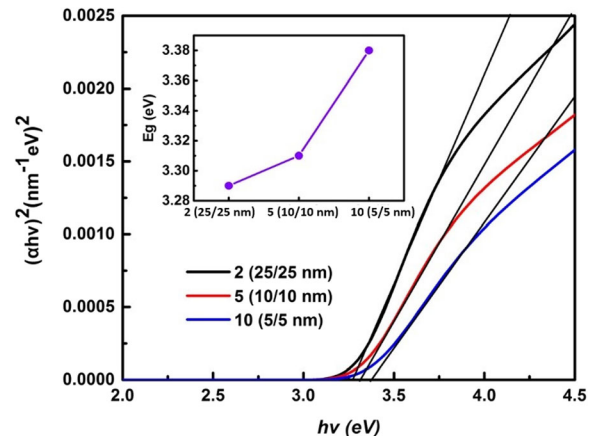

Fig. 7 Evaluated optical bandgap of nanolaminates with different bilayer thicknesses

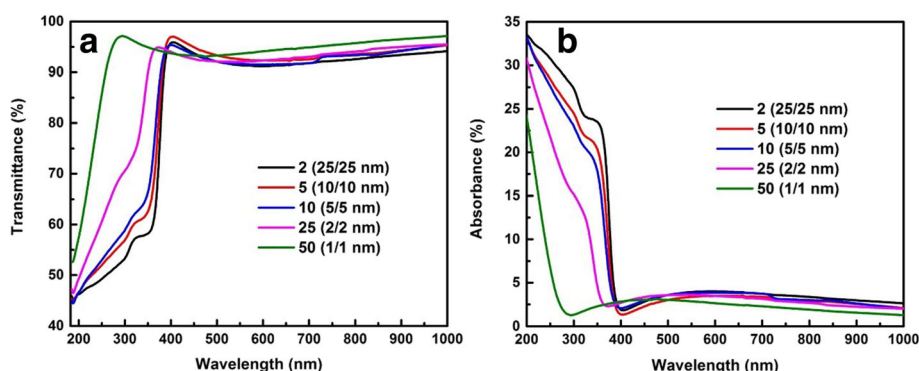Li et al. Nanoscale Research Letters (2017) 12:563

Page 7 of 9

Fig. 8 a Transmittance and **b** absorbance spectra of nanolaminates grown on quartz substrates with different bilayer thicknesses

25 (2/2 nm) and 50 (1/1 nm), the quantum confinement effect becomes dominant, and the interfacial reaction intensifies which makes the nanolaminates show the characteristics of Al_2O_3 gradually. At this point, the blue shift is the total contribution of the BM effect, the quantum confinement effect, and the characteristic evolution of nanolaminates. That is to say, these three factors cause the enormous shift of the absorption edge. As a whole, the absorption edge can be modulated by the bilayer thickness in the ultraviolet region (200–400 nm). According to this, it can be applied as ultraviolet detector. Besides, all of the Al_2O_3/ZnO nanolaminates show a transmittance above 90% in visible and near-infrared region, along with a sharp absorption band edge. The transmittance here shows nearly similar value and trend with that of many other TCO materials [36], which makes it possible to be applied as TCO material.

Electrical Properties

The Hall effect measurement is conducted to correlate the analyses with the electrical properties of the Al_2O_3/ZnO nanolaminates. Nanolaminates prepared on quartz substrates are selected as the test samples to remove the spatial resistivity distribution, and Fig. 9 displays the testing results. At the beginning, the carrier concentration and resistivity show little change and remain at around 10^{19} cm^{-3} and 10^{-2}Ω cm, respectively. With decreasing bilayer thickness, the carrier concentration sharply drops and the resistivity increases as well. It can be interpreted by the interfacial reaction of Al_2O_3/ZnO layers which results in the characteristic evolution of nanolaminates. The nanolaminates show insulation characteristic of Al_2O_3 gradually and realize the tunableness of resistivity by changing their bilayer thickness. In addition, the values of the carrier concentration of nanolaminates 2 (25/25 nm), 5 (10/10 nm), and 10 (5/5 nm) are 4.99×10^{19}, 5.26×10^{19}, and 8.91×10^{19} cm^{-3}, respectively. It shows a slow growth in accordance with the explanation of the bandgap results, and the values

approximately equal to those of TCO materials from the results of other reports [25, 37]. So these three kinds of nanolaminates possess not only favorable electrical conductivity but also excellent light transmittance in the visible and near-infrared region. It is vital for Al_2O_3/ZnO nanolaminates to play a role in the field of transparent conductor. The samples 25 (2/2 nm) and 50 (1/1 nm) present insulation characteristic and realize the tunableness of resistivity, which can be applied as high-resistivity layer in semiconductor devices.

Conclusions

We have investigated the morphological, optical, and electrical properties of Al_2O_3/ZnO nanolaminates among various bilayer thicknesses ranging from 2 to 50 nm. The clear layer boundaries and low surface roughness show high-quality morphologies of nanolaminates prepared by ALD method. With the decrease of the bilayer thickness, inserted Al_2O_3 layers in nanolaminates begin to limit the roughness, which leads to the nanolaminates more smooth. When the bilayer thickness reaches a certain value, this roughness
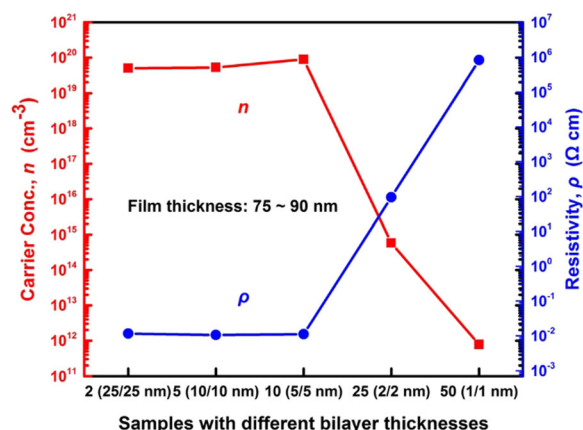

Fig. 9 Carrier concentration and resistivity of nanolaminates grown on quartz substrate with different bilayer thicknesses

Li *et al. Nanoscale Research Letters* (2017) 12:563

Page 8 of 9

limitation can be ignored. The thickness, optical constants, and bandgap information of nanolaminates have been extracted from SE analysis. With decreasing bilayer thickness, the absorption edge of extinction coefficient has a blue shift, and the optical band gap energies show a growing trend, because the BM effect, the quantum confinement effect, and the characteristic evolution of nanolaminates have significant influence on them. This blue shift also occurs in the transmission and absorbance spectra with high transmittance beyond 90% in the visible and near-infrared region. Moreover, by varying the bilayer thickness, the electrical properties also show two kinds of characteristics, and the modulation of characteristics is realized. The nanolaminates 2 (25/25 nm), 5 (10/10 nm), and 10 (5/5 nm) show high carrier concentration above 10^{19} cm^{-3}, which can be applied as transparent conductive material. And also, the nanolaminates 25 (2/2 nm) and 50 (1/1 nm) possessing high resistivity can be used as high-resistivity layer in semiconductor manufacturing process.

Abbreviations
AFM: Atomic force microscopy; ALD: Atomic layer deposition; AZO: Al-doped ZnO; BM: Burstein-Moss; DEZ: Diethylzinc; FB: Forouhi-Bloomer; RMSE: Root-mean-square error; SE: Spectroscopic ellipsometry; TCO: Transparent conductive oxide; TEM: Transmission electron microscope; TMA: Trimethylaluminum

Authors' contributions
DHL and CHZ performed the experiments and drafted the manuscript. WCZ provided helpful discussions. QHL, LW, HZ, and LC participated in the design and coordination of the study. XC and RJZ proposed the initial work and finalized the manuscript, and RJZ supervised the work at the same time. All authors read and approved the final manuscript.

Competing interests
The authors declare that they have no competing interests.

Publisher's Note
Springer Nature remains neutral with regard to jurisdictional claims in published maps and institutional affiliations.

Author details
[1]Key Laboratory of Micro and Nano Photonic Structures, Ministry of Education, Department of Optical Science and Engineering, Fudan University, Shanghai 200433, China. [2]State Key Laboratory of Applied Optics, Changchun Institute of Optics, Fine Mechanics and Physics, Chinese Academy of Sciences, Changchun, Jilin 130033, China. [3]Institute of Electronic Engineering, China Academy of Engineering Physics, Mianyang, Sichuan 621999, China. [4]National Laboratory for Infrared Physics, Shanghai Institute of Technical Physics, Chinese Academy of Sciences, Shanghai 200083, China.

References
1. Rowlette PC, Wolden CA (2010) Pulsed plasma-enhanced chemical vapor deposition of Al₂O₃–TiO₂ nanolaminates. Thin Solid Films 518:3337–3341
2. Seo SW, Jung E, Chae H, Cho SM (2012) Optimization of Al₂O₃/ZrO₂ nanolaminate structure for thin-film encapsulation of OLEDs. Org Electron 13:2436–2441
3. Richardson JJ, Björnmalm M, Caruso F (2015) Multilayer assembly. Technology-driven layer-by-layer assembly of nanofilms. Science 348: aaa2491
4. Li J, Bi X (2016) Temperature- and frequency-dependent dielectric behaviors of insulator/semiconductor (Al₂O₃/ZnO) nanolaminates with various ZnO thicknesses. J Phys D Appl Phys 49:285301
5. Lackner JM, Waldhauser W, Major R, Hartmann P (2013) Biomimetics in thin film design—wrinkling and fracture of pulsed laser deposited films in comparison to human skin. Surf Coat Technol 215:192–198
6. Raghavan R, Bechelany M, Parlinska M, Frey D (2012) Nanocrystalline-to-amorphous transition in nanolaminates grown by low temperature atomic layer deposition and related mechanical properties. Appl Phys Lett 100:191912
7. Karvonen L, Saynatjoki A, Chen Y, Jussila H, Ronn J, Ruoho M, Alasaarela T, Kujala S, Norwood RA, Peyghambarian N (2013) Enhancement of the third-order optical nonlinearity in ZnO/Al₂O₃ nanolaminates fabricated by atomic layer deposition. Appl Phys Lett 103:031903
8. Elias J, Bechelany M, Utke I, Erni R, Hosseini D, Michler J, Philippe L (2012) Urchin-inspired zinc oxide as building blocks for nanostructured solar cells. Nano Energy 1:696–705
9. Allan-Wojtas P, Hildebrand PD, Braun PG, Smith-King HL, Carbyn S, Renderos WE (2011) Highly active oxide photocathode for photoelectrochemical water reduction. Nat Mater 10:456–461
10. Jędrzejewska-Szczerska M, Wierzba P, Chaaya AA, Bechelany M, Miele P, Viter R, Mazikowski A, Karpienko K, Wróbel M (2015) ALD thin ZnO layer as an active medium in a fiber-optic Fabry–Perot interferometer. Sensor Actuat A-Phys 221:88–94
11. Viter R, Iatsunskyi I, Fedorenko V, Tumenas S, Balevicius Z, Ramanavicius A, Balme S, Kempiński M, Nowaczyk G, Jurga S, Bechelany M (2016) Enhancement of electronic and optical properties of ZnO/Al₂O₃ nanolaminates coated electrospun nanofibers. J Phys Chem C 120:5124–5132
12. Baitimirova M, Viter R, Andzane J, Lee A, Voiry D, Iatsunskyi I, Coy E, Mikoliunaite L, Tumenas S, Zaleski K, Balevicius Z, Baleviciute I, Ramanaviciene A, Ramanavicius A, Jurga S, Erts D, Bechelany M (2016) Tuning of structural and optical properties of graphene/ZnO nanolaminates. J Phys Chem C 120:23716–23725
13. Benhaoua B, Rahal A, Benramache S (2014) The structural, optical and electrical properties of nanocrystalline ZnO:Al thin films. Superlattices Microst 68:38–47
14. Lee DJ, Kim HM, Kwon JY, Choi H, Kim SH, Kim KB (2011) Structural and electrical properties of atomic layer deposited Al-doped ZnO films. Adv Funct Mater 21:448–455
15. Schulze K, Maennig B, Leo K, Tomita Y (2007) Organic solar cells on indium tin oxide and aluminum doped zinc oxide anodes. Appl Phys Lett 91:073521
16. Meyer J, Hamwi S, Johannes HH, Riedl T, Kowalsky W (2008) Indium-free transparent organic light emitting diodes with Al doped ZnO electrodes grown by atomic layer and pulsed laser deposition. Appl Phys Lett 93:073308
17. Zheng H, Zhang RJ, Xu JP, Wang S, Zhang T, Sun Y, Zheng YX, Wang SY, Chen X, Chen LY (2016) Thickness-dependent optical constants and annealed phase transitions of ultrathin ZnO films. J Phys Chem C 120: 22532–22538
18. Kim LH, Jeong YJ, An TK, Park S, Jang JH, Nam S, Jang J, Kim SH, Park CE (2015) Optimization of Al₂O₃/TiO₂ nanolaminate thin films prepared with different oxide ratios, for use in organic light-emitting diode encapsulation, via plasma-enhanced atomic layer deposition. Phys Chem Chem Phys 18: 1042–1049
19. Marichy C, Bechelany M, Pinna N (2012) ChemInform abstract: atomic layer deposition of nanostructured materials for energy and environmental applications. Adv Mater 24:1017–1032
20. Na JS, Peng Q, Scarel G, Parsons GN (2009) Role of gas doping sequence in surface reactions and dopant incorporation during atomic layer deposition of Al-doped ZnO. Chem Mater 21:5585–5593
21. Chaaya AA, Viter R, Baleviciute I, Bechelany M, Ramanavicius A, Gertnere Z, Erts D, Smyntyna V, Miele P (2016) Tuning optical properties of Al₂O₃/ZnO nanolaminates synthesized by atomic layer deposition. J Phys Chem C 118: 3811–3819
22. Viter R, Baleviciute I, Chaaya AA, Mikoliunaite L, Balevicius Z, Ramanavicius A, Zalesska A, Vataman V, Smyntyna V, Gertnere Z (2015) Optical properties of ultrathin Al₂O₃/ZnO nanolaminates. Thin Solid Films 594:96–100

Li *et al. Nanoscale Research Letters* (2017) 12:563

Page 9 of 9

23. López J, Martínez J, Abundiz N, Domínguez D, Murillo E, Castillón FF, Machorro R, Farías MH, Tiznado H (2016) Thickness effect on the optical and morphological properties in Al_2O_3/ZnO nanolaminate thin films prepared by atomic layer deposition. Superlattices Microst 90:265–273

24. Elam JW, Sechrist ZA, George SM (2002) ZnO/Al_2O_3 nanolaminates fabricated by atomic layer deposition: growth and surface roughness measurements. Thin Solid Films 414:43–55

25. Zhai CH, Zhang RJ, Chen X, Zheng YX, Wang SY, Liu J, Dai N, Chen LY (2016) Effects of Al doping on the properties of ZnO thin films deposited by atomic layer deposition. Nanoscale Res Lett 11:407

26. Ott AW, Klaus JW, Johnson JM, George SM (2009) Erratum to "Al_2O_3 thin film growth on Si (100) using binary reaction sequence chemistry". Thin Solid Films 292:135–144

27. Xu JP, Zhang RJ, Zhang Y, Wang ZY, Chen L, Huang QH, Lu HL, Wang SY, Zheng YX, Chen LY (2016) The thickness-dependent band gap and defect features of ultrathin ZrO2 films studied by spectroscopic ellipsometry. Phys Chem Chem Phys 18:3316–3321

28. Li DH, Zheng H, Wang ZY, Zhang RJ, Zhang H, Zheng YX, Wang XY, Zhang W, Chen LY (2017) Dielectric functions and critical points of crystalline WS_2 ultrathin films with tunable thickness. Phys Chem Chem Phys 19:12022–12031

29. Forouhi AR, Bloomer II (1986) Optical dispersion relations for amorphous semiconductors and amorphous dielectrics. Phys Rev B 34:7018

30. Forouhi AR, Bloomer II (1986) Optical properties of crystalline semiconductors and dielectrics. Phys Rev B 38:1865

31. López J, Solorio E, Borbón-Nuñez HA, Castillón FF, Machorro R, Nedev N, Farías MH, Tiznado H (2017) Refractive index and bandgap variation in Al_2O_3-ZnO ultrathin multilayers prepared by atomic layer deposition. J Alloys Compd 691:308–315

32. Li QH, Zhu D, Liu W, Liu Y, Ma XC (2008) Optical properties of Al-doped ZnO thin films by ellipsometry. Appl Surf Sci 254:2922–2926

33. Fujiwara H, Kondo M (2005) Effects of carrier concentration on the dielectric function of ZnO:Ga and In_2O_3:Sn studied by spectroscopic ellipsometry: analysis of free-carrier and band-edge absorption. Phys Rev B 71:075109

34. Burstein E (1954) Anomalous optical absorption limit in InSb. Phys Rev 93:632–633

35. Liu Y, Li Q, Shao H (2009) Optical and photoluminescent properties of Al-doped zinc oxide thin films by pulsed laser deposition. J Alloys Compd 485:529–531

36. Mendezgamboa JA, Castrorodriguez R, Perezquintana IV, Medinaesquivel RA, Martelarbelo A (2016) A figure of merit to evaluate transparent conductor oxides for solar cells using photonic flux density. Thin Solid Films 599:14–18

37. Pradhan AK, Mundle RM, Santiago K, Skuza JR, Xiao B, Song KD, Bahoura M, Cheaito R, Hopkins PE (2014) Extreme tunability in aluminum doped zinc oxide plasmonic materials for near-infrared applications. Sci Rep 4:6415–6420